

# Interplay between ferroic orders at the FeRh/BaTiO<sub>3</sub> interfaces

Viktoria V. Ivanovskaya,<sup>1,\*</sup> Alberto Zobelli,<sup>2</sup> Alexandre Gloter,<sup>2</sup> Manuel Bibes,<sup>1</sup> and Agnès Barthélémy<sup>1</sup>

<sup>1</sup>*Unité Mixte de Physique CNRS-Thales, 1 Avenue Augustin Fresnel,  
91767 Palaiseau, France and Université Paris-Sud, 91405 Orsay, France*

<sup>2</sup>*Laboratoire de Physique des Solides, Université Paris-Sud, CNRS UMR 8502, F-91405, Orsay, France*

It has been recently demonstrated that the magnetic state of FeRh can be controlled by electric fields in FeRh/BaTiO<sub>3</sub> heterostructures [R.O. Cherifi *et al.* Nature Mater. **13**, 345 (2014)]. Voltage-controlled changes in the ferroelastic domain structure of BaTiO<sub>3</sub> appeared to drive this effect, with charge accumulation and depletion due to ferroelectricity playing a more elusive role. To make this electric-field control of magnetic order non-volatile, the contribution of ferroelectric field-effect must be further enhanced, which requires understanding the details of the interface between FeRh and BaTiO<sub>3</sub>. Here we report on the atomic structure and electron screening at this interface through density functional theory simulations. We relate different screening capabilities for the antiferromagnetic and ferromagnetic states of FeRh to different density of states at the Fermi level of corresponding bulk structures. We predict that the stability of the ferroelectric state in adjacent very thin BaTiO<sub>3</sub> films will be affected by magnetic order in FeRh. This control of ferroelectricity by magnetism can be viewed as the reciprocal effect of the voltage-controlled magnetic order previously found for this system.

## I. INTRODUCTION

The equilibrium ordered *bcc* B2 FeRh alloy exhibits a first-order antiferromagnetic (AFM) to ferromagnetic (FM) phase transition slightly above room temperature.<sup>1,2</sup> Recent achievements in the preparation of ordered alloy thin films combined with their potential technological applications (heat assisted magnetic recording or microelectromechanical devices, etc.) have stimulated a renewed interest for this material.<sup>3–13</sup> Experimentally it has been shown that in thin films the AFM to FM transition is highly sensitive to the film thickness and composition, heat treatment, magnetic field, pressure, etc.<sup>14–22</sup>

The capability to electrically switch the magnetic state of FeRh at a limited energy cost makes this material of the highest interest for potential spintronic applications. Very recently it has been demonstrated that in FeRh/BaTiO<sub>3</sub> heterostructures a moderate electric field changing the BaTiO<sub>3</sub> ferroelastic state can produce a giant magnetization variation resulting from an AFM to a FM first order transition in the FeRh slab.<sup>23</sup> The effect occurs just above room temperature and it is mostly driven by voltage-induced strain from the BaTiO<sub>3</sub> substrate transferred to the FeRh. This effect appears to affect the FeRh film, but it has been suggested that an additional contribution to the magnetic phase transition may arise from more local interface effects due to charge accumulation and depletion.<sup>23</sup>

To make the voltage-induced change in the magnetic order non-volatile, such electronic effects must be made dominant over strain effects, which requires a detailed understanding of the subtle interplay between magnetism and the local electronic structure at the FeRh/BaTiO<sub>3</sub> interface. This is also especially important for future tunneling devices based on ferroelectric barriers and metamagnetic compounds such as FeRh as electrode. A common difficulty encountered while working with ferroelec-

tric tunnel junctions is the preservation of ferroelectricity at the very low thickness of a tunnel barrier.<sup>24,25</sup> Such constrain was not present in Ref.<sup>23</sup> where FeRh films were grown onto BaTiO<sub>3</sub> substrate. An accurate description of the atomic structure of multiferroic thin film interfaces combined to an analysis of local electronic structure and screening at the metal electrodes is thus required to optimize their design.

In the present work we report the local electronic structure and electron screening at FeRh/BaTiO<sub>3</sub> interfaces obtained through density functional theory simulations. We show that different density of states at the Fermi level of bulk structures yield different screening capabilities for the AFM and FM phases. This effect is then related to the critical thickness of the metal electrodes in order to stabilize the ferroelectric polarization.

## II. COMPUTATIONAL DETAILS

Spin-polarized density functional calculations were performed under the local density approximation as implemented in the AIMPRO code.<sup>26,27</sup> Relativistic pseudo-potentials were generated using the Hartwingster-Goedecker-Hutter scheme.<sup>28</sup> As basis sets, 50 independent Gaussian functions were used for iron and rhodium, 40 for titanium and oxygen and 20 for barium atoms. All atoms in a supercell were optimized using a conjugate gradient scheme, starting from the ferromagnetic or, alternatively, from the antiferromagnetic configuration in the FeRh slab, until the forces become less than 10<sup>-4</sup> eV/Å. Electronic structure convergence was ensured for each supercell by using a 9 × 9 × 1 k points mesh generated from a Monkhorst-Pack set sampling of the Brillouin zone<sup>29</sup> and constraining the energy difference in the self-consistent cycle to be below 10<sup>-7</sup> Hartree.

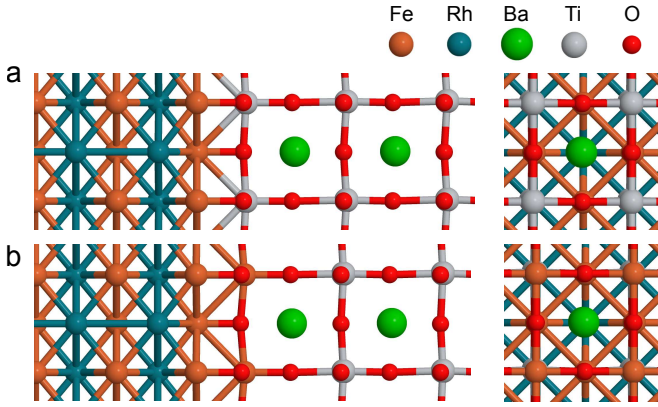


Figure 1. Atomic model of the FeRh/BaTiO<sub>3</sub> interface with (a) Fe interface plane and (b) FeO<sub>2</sub> interface plane.

### III. RESULTS AND DISCUSSION

Atomic models have been built in a supercell approach considering 4.5 or 6.5 unit cells for the metal slabs and 5.5, 7.5 or 11.5 unit cells for the perovskite slab, following the epitaxial relationship (001)FeRh||(001)BaTiO<sub>3</sub>:[100]FeRh||[110]BaTiO<sub>3</sub>. We considered FeRh slabs terminated by both Fe- or FeO<sub>2</sub>-planes at the interface with BaTiO<sub>3</sub> (note, that an FeO<sub>2</sub>-type termination was found for the Fe/BaTiO<sub>3</sub> interface<sup>30</sup>). In the Fe- terminated structure, metal atoms are located on top of the oxygen atoms of the perovskite surface (Fig. 1.a). From this configuration, the FeO<sub>2</sub>- terminated structure can be obtained by substituting in the -TiO<sub>2</sub> interfacial plane Ti by Fe leading to a further iron enrichment (Fig. 1.b). The two interfaces within the supercell have the same composition but different orientations with respect to the ferroelectric polarization, towards ( $P_{\text{up}}$ ) or away from the interface ( $P_{\text{down}}$ ). In our simulations the FeRh in-plane cell parameter<sup>31</sup> was constrained to that of BaTiO<sub>3</sub> (in our model 3.95Å, obtained from bulk cell optimization) while the supercell out-of-plane parameter was free to relax. For the bulk FeRh structure, imposing epitaxy on the BaTiO<sub>3</sub> substrate, one leads to a tetragonal phase with the atomic and magnetic ordering of the FeRh alloy preserved, and a  $c/a$  ratio of 1.15 for the AFM phase and 1.16 for the FM phase. These values differ from those of the bulk *bcc* B2 phase but are very close to the experimental  $c/a$  ratio of the L1<sub>0</sub> phase.<sup>32,33</sup>

Similarly to what was observed for the cubic phase under hydrostatic compression,<sup>34,35</sup> lattice distortions due to strain lead to only a slight decrease of the magnetization at the cubic to tetragonal phase transition. In the *bcc* B2 structure, magnetic moments on the Fe and Rh atoms are respectively 3.21 and 0.00  $\mu\text{B}$  in the AFM phase and 3.29 and 0.94  $\mu\text{B}$  in FM phase, consistent with previous first-principles simulations.<sup>34–36</sup> In the tetragonal structure promoted by the BaTiO<sub>3</sub> substrate we obtain for Fe and Rh atoms 3.07  $\mu\text{B}$  and 0.0  $\mu\text{B}$  in the AFM phase

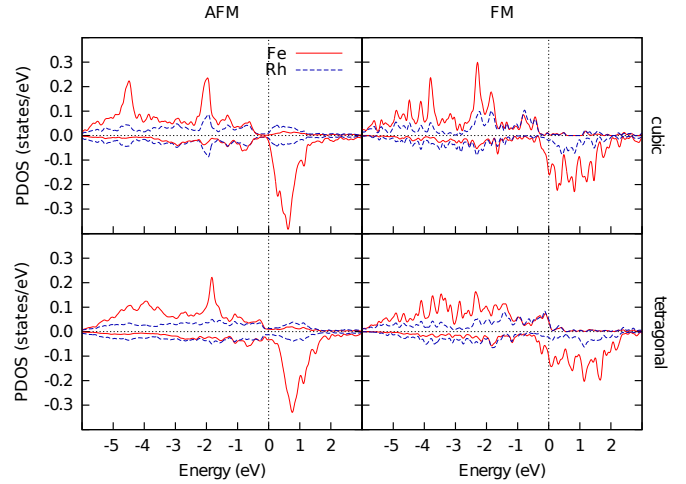


Figure 2. Spin resolved Fe 3d and Rh 4d partial densities of states for AFM and FM FeRh in cubic (top) and tetragonal (bottom) phases. Fermi level is set at zero.

and 3.16  $\mu\text{B}$  and 0.71  $\mu\text{B}$  in the FM phase. This trend is consistent with experimental findings on somewhat lower magnetization in the tetragonal FeRh phase as compared to the cubic one.<sup>37</sup>

We first discuss the stability of ferroelectricity in BaTiO<sub>3</sub> in the FeRh/BaTiO<sub>3</sub> system with Fe- plane termination as a function of metal electrode thickness. It is well known that in ultrathin ferroelectric films strong depolarizing fields tend to suppress ferroelectricity and drive the system into a paraelectric state. For instance, it has been calculated that the critical thickness for BaTiO<sub>3</sub> is 7 unit cells when interfaced with SrRuO<sub>3</sub>.<sup>24</sup> However, this result can not be generalized to different heterostructures since critical thicknesses are affected by the specific screening lengths of the chosen metal electrodes. Furthermore, the thickness of the metal is seldom discussed as an additional parameter influencing the ferroelectric stability, while it can have a strong influence for very thin electrodes.

For FeRh electrodes, FM or AFM states should be considered as separated cases due to their different electronic properties that can be further modified by the tetragonal distortions imposed by BaTiO<sub>3</sub>. Looking at the spin resolved partial densities of states (PDOS) projected at Fe and Rh sites (Fig. 2), the AFM FeRh in the cubic phase has a low density of states at the Fermi level which is only slightly increased when the system becomes tetragonal. The cubic FM FeRh has a high density of minority spins at the Fermi level with a spin polarization that is reduced in the tetragonal structure. The overall lower density of states at the Fermi level for AFM FeRh compared to FM FeRh is preserved both in the cubic and tetragonal phases. In both crystal structures, the density of states at the Fermi level is thus very different for the AFM and FM phases, consistent with experimental findings.<sup>7,8</sup> FeRh thus has a different capability for charge accumulation or depletion depending on its magnetic state. As

a consequence, higher screening lengths and thus higher depolarization fields are expected at AFM FeRh interfaces in contrast to FM FeRh interfaces.

In Fig. 3 we present the amplitude of the Ti-O displacements at  $\text{TiO}_2$  planes (whose values are related to the ferroelectric polarization) as a function of the  $\text{BaTiO}_3$  and FeRh slab thicknesses for FM and AFM magnetic states. In a previous study, the critical thickness for  $\text{BaTiO}_3$  slabs has been evaluated in about 18 Å (4.5 unit cells) for 13 Å thick Fe electrodes (9 Fe planes).<sup>38</sup> Using similar ferroelectric and metal slabs thicknesses for the FeRh case, we find that Ti-O displacements in the middle section of the  $\text{BaTiO}_3$  slab approach the bulk value (0.12 Å) only when the FeRh electrode is in the FM magnetic state. A low rumpling and a loss of polarization (corresponding to about the half of the bulk displacements) is instead associated to the FeRh AFM magnetic state. This effect occurs even for thicker  $\text{BaTiO}_3$  slabs (30 Å and 40 Å) for which depolarizing fields are lower. The critical thickness of  $\text{BaTiO}_3$  to preserve the ferroelectricity should occur above 40 Å for AFM FeRh electrodes while it is less than 20 Å for FM FeRh electrodes. In other words, the ferroelectric polarization of a  $\text{BaTiO}_3$  film with a thickness between 20 and 40 Å can be controlled by switching the magnetic state of the adjacent thin FeRh slab. This behavior can be viewed as a reciprocal effect of the voltage controlled magnetic order observed for such heterostructures.<sup>23</sup> Finally, for all structures considered we observe a higher rumpling of the polarization at the  $P_{\text{up}}$  interface compared to the  $P_{\text{down}}$  interface.

The low Ti-O displacements observed for AFM FeRh interfaces are a consequence of the strong residual depolarizing fields due to incomplete charge screening. We evaluate charges for bulk and interface structures through a Mulliken population analysis (Tab. I and Fig. 4). In bulk FeRh we obtain a charge transfer of  $+0.71 e$  from Rh to Fe for the AFM and  $+0.69 e$  for the FM magnetic configurations (Tab. I). Considering the  $\text{BaTiO}_3$  slab in the paraelectric state (mirror symmetry imposed), iron is further positively charged at the interface due to its partial oxidation. For the  $\text{BaTiO}_3$  ferroelectric state, the polarization screening varies the charge state at the  $P_{\text{up}}$  and  $P_{\text{down}}$  interfaces. For the  $P_{\text{up}}$  interface a higher electron accumulation at the first Fe plane occurs for FM FeRh compared to AFM FeRh (Tab. I).

Besides the first interfacial Fe plane, in Fig. 4 we represent the difference of charge with respect to bulk charge states for the whole heterostructures. In the case of FM FeRh the carrier density is high enough to provide a screening length of the order of only a few surface metal layers (Fig. 4). For AFM FeRh, which is a worst metal as we discussed above, this length increases significantly and for thin metal layers it becomes of the same order of magnitude as the electrode thickness. A way to reduce the critical thickness for the ferroelectric can be achieved through a better screening by increasing the metal thickness. This explains the different critical thicknesses ob-

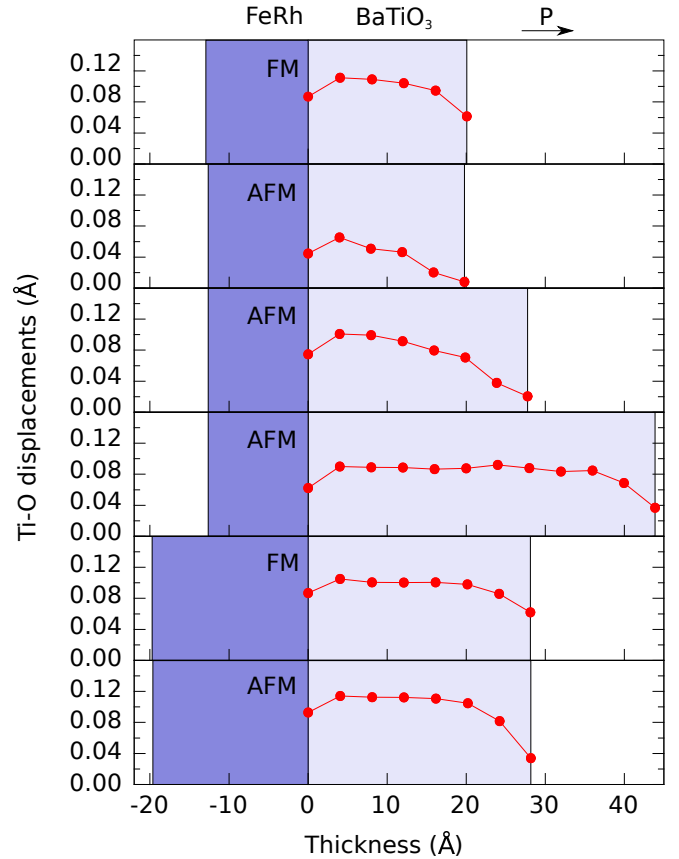


Figure 3. Displacements of Ti atoms related to the O atoms at  $\text{TiO}_2$ -planes for heterostructures with different FM and AFM FeRh and  $\text{BaTiO}_3$  thicknesses (red curves). The thicknesses of ferroelectric and metallic slabs are marked by rectangles. The arrow shows the direction of the polarization in the ferroelectric slab.

served for the two magnetic phases (Figure 3).

We should consider also that the ferroelectric polarization in the presence of AFM FeRh slabs promotes a local transition to the FM phase solely of the first interfacial unit cell. Whereas bulk FM FeRh is 93 meV higher in energy than AFM FeRh, we find that this local mag-

Table I. Fe charge in bulk FeRh and charge difference from the bulk charge for Fe atoms at the first atomic plane of the FeRh/ $\text{BaTiO}_3$  interface.

	Fe charge reference ( $e/\text{atom}$ )	
	FM	AFM
Bulk FeRh	0.71	0.69
	Fe $\Delta$ charge at the interface plane ( $e/\text{atom}$ )	
	FM	AFM
$\text{BaTiO}_3$ , paraelectric	0.16	0.16
$\text{BaTiO}_3$ , $P_{\text{up}}$ interface	0.11	0.13
$\text{BaTiO}_3$ , $P_{\text{down}}$ interface	0.17	0.17

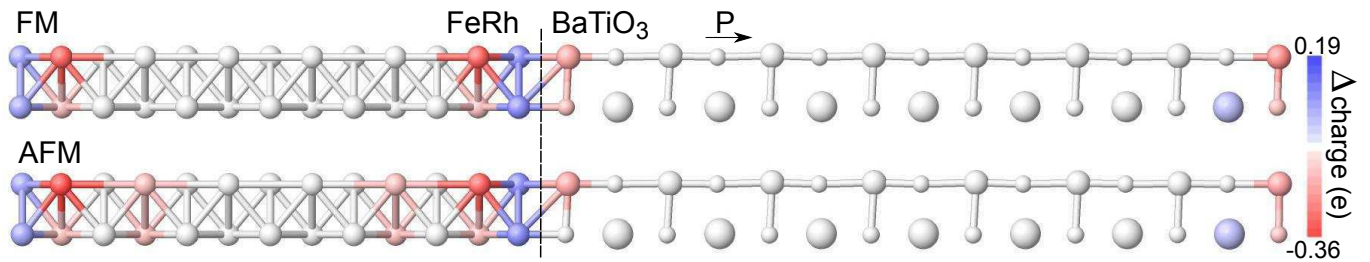


Figure 4. Differential charge distribution for the FM (top) and AFM (bottom) FeRh/BaTiO<sub>3</sub> heterostructures. Charges are calculated as the difference between the induced charges at the interfaces and their bulk counterparts; the polarization direction is indicated by the arrow.

netic switch at the  $P_{\text{up}}$  interface lead to an energy gain of 100 meV per interface unit cell. Nevertheless, this more complex magnetic state does not affect trends in ferroelectric polarizations discussed above. However, the application of an electric field or the use of a ferroelectric with a higher polarization should promote this interfacial AFM to FM transition in a bigger volume close to the interface. This can have important consequences for spin-dependent transport in multiferroic tunnel junctions based on FeRh.

Finally, we comment on screening effects in the presence of a FeRh oxidized interface i.e. with a FeO<sub>2</sub>– interfacial plane. Charges in this last plane contribute also to the screening. In the above considered unoxidized case, there is a charge accumulation of  $-0.71 e$  for  $P_{\text{down}}$  and  $-0.82 e$  for  $P_{\text{up}}$  at the terminal TiO<sub>2</sub>– plane (Fig. 4). In the oxidized case, the FeO<sub>2</sub>– plane has a ferromagnetic order and the charge state is  $-0.91 e$  at the  $P_{\text{down}}$  interface and  $-1.05 e$  at the  $P_{\text{up}}$  interface, which results in an enhanced screening. Thus, charge accumulation at the successive FeRh planes is reduced and in this case the system in the AFM state is not further stabilized by switching the first unit cell to the FM state.

#### IV. CONCLUSIONS

In this paper, via density functional theory simulations we have provided insights on the role of the electrode magnetic state in stabilizing the ferroelectric polarization for the FeRh/BaTiO<sub>3</sub> system. In particular, we have shown that screening is higher for FM FeRh than AFM FeRh. This behavior is in agreement with the differences on the near Fermi energy density of states of the two magnetic phases observed in both cubic and tetragonal bulk

lattices: AFM FeRh can be described as a worst metal than FM FeRh. For thin FeRh/BaTiO<sub>3</sub> heterostructures the thicknesses of both the ferroelectric and ferromagnetic layers contribute to the stability of the ferroelectric phase. Indeed at a given ferroelectric thickness, associated with a specific depolarizing field, it is possible to define a critical thickness of the ferromagnetic electrode below which the screening is incomplete. The different screening capabilities of the FM FeRh and AFM FeRh phases lead then to different critical thicknesses.

In a previous work<sup>23</sup> we presented experimental evidences for a control of the FeRh magnetic state in the FeRh/BaTiO<sub>3</sub> heterostructure through the BaTiO<sub>3</sub> ferroelectric polarization. The theoretical results presented here suggest a mechanism where the switch between magnetic states of a thin FeRh electrode would lead to complete or uncomplete screening and thus to changes in the ferroelectric polarization (and possibly Curie temperature) of the BaTiO<sub>3</sub>. This mechanism should be general, which suggests that changes in the ferroelectric properties should occur in heterostructures combining a ferroelectric with a material hosting phases with different densities of states. Such systems are ubiquitous in the perovskite family (for instance manganites or nickelates with sharp metal-insulator transitions<sup>39–41</sup>) that could be easily combined with BaTiO<sub>3</sub> or other ferroelectrics.

#### ACKNOWLEDGMENTS

This work received financial support from the French Agence Nationale de la Recherche through project NOMILOPS (ANR-11-BS10-0016) and the European Research Council Advanced Grant FEMMES (contract no. 267579). We would like to thank L.C. Philips for useful comments.

\* v.ivanovskaya@gmail.com

<sup>1</sup> M. Fallot, Ann. Phys. **10**, 291 (1938).

<sup>2</sup> L. Muldower and F. de Bergevin, J. Chem. Phys. **35**, 1904 (1961).

<sup>3</sup> R. Fan, C. Kinane, T. Charlton, R. Dorner, M. Ali, M. de Vries, R. Brydson, C. Marrows, B. Hickey, D. Arena, *et al.*, Phys. Rev. B **82**, 184418 (2010).

- <sup>4</sup> C. Bordel, J. Juraszek, D. W. Cooke, C. Baldasseroni, S. Mankovsky, J. Minár, H. Ebert, S. Moyerman, E. Fullerton, and F. Hellman, *Phys. Rev. Lett.* **109**, 117201 (2012).
- <sup>5</sup> D. W. Cooke, F. Hellman, C. Baldasseroni, C. Bordel, S. Moyerman, and E. E. Fullerton, *Phys. Rev. Lett.* **109**, 255901 (2012).
- <sup>6</sup> M. Loving, F. Jimenez-Villacorta, B. Kaeswurm, D. A. Arena, C. H. Marrows, and L. H. Lewis, *J. Phys. D: Appl. Phys.* **46**, 162002 (2013).
- <sup>7</sup> M. de Vries, M. Loving, A. Mihai, L. Lewis, D. Heiman, and C. Marrows, *New J. Phys.* **15**, 013008 (2013).
- <sup>8</sup> A. X. Gray, D. W. Cooke, P. Krüger, C. Bordel, A. M. Kaiser, S. Moyerman, E. E. Fullerton, S. Ueda, Y. Yamashita, A. Gloskovskii, *et al.*, *Phys. Rev. Lett.* **108**, 257208 (2012).
- <sup>9</sup> T. Miyanaga, T. Itoga, T. Okazaki, and K. Nitta, *J. Phys.: Conf. Ser.* **190**, 012097 (2009).
- <sup>10</sup> S. Inoue, N. N. Phuoc, J. Cao, N. T. Nam, H. Y. Y. Ko, and T. Suzuki, *J. Appl. Phys.* **103**, 07B312 (2008).
- <sup>11</sup> E. Mancini, F. Pressacco, M. Haertinger, E. E. Fullerton, T. Suzuki, G. Woltersdorf, and C. H. Back, *J. Phys. D: Appl. Phys.* **46**, 245302 (2013).
- <sup>12</sup> C. Baldasseroni, C. Bordel, A. Gray, A. Kaiser, F. Kronast, J. Herrero-Albillos, C. Schneider, C. Fadley, and F. Hellman, *Appl. Phys. Lett.* **100**, 262401 (2012).
- <sup>13</sup> J.-S. Lee, E. Vescovo, L. Plucinski, C. M. Schneider, and C.-C. Kao, *Phys. Rev. B* **82**, 224410 (2010).
- <sup>14</sup> G. C. Han, J. J. Qiu, Q. Yap, P. Luo, T. Kanbe, T. Shige, D. E. Laughlin, and J.-G. Zhu, *J. Appl. Phys.* **113**, 123909 (2013).
- <sup>15</sup> J. Kim, P. Ryan, Y. Ding, L. Lewis, M. Ali, C. Kinane, B. Hickey, C. Marrows, and D. Arena, *Appl. Phys. Lett.* **95**, 222515 (2009).
- <sup>16</sup> G. C. Han, J. J. Qiu, Q. Yap, P. Luo, D. E. Laughlin, J.-G. Zhu, T. Kanbe, and T. Shige, *J. Appl. Phys.* **113**, 17C107 (2013).
- <sup>17</sup> J. Van Driel, R. Coehoorn, G. Strijkers, E. Bruck, and F. De Boer, *J. Appl. Phys.* **85**, 1026 (1999).
- <sup>18</sup> J. Cao, N. T. Nam, S. Inoue, H. Y. Y. Ko, N. N. Phuoc, and T. Suzuki, *J. Appl. Phys.* **103**, 07F501 (2008).
- <sup>19</sup> I. Suzuki, T. Koike, M. Itoh, T. Taniyama, and T. Sato, *J. Appl. Phys.* **105**, 07E501 (2009).
- <sup>20</sup> A. Hillion, A. Cavallin, S. Vlaic, A. Tamion, F. Tournus, G. Khadra, J. Dreiser, C. Piamonteze, F. Notling, S. Rusponi, K. Sato, T. J. Konno, O. Proux, and H. Dupuis, V. Brune, *Phys. Rev. Lett.* **110**, 087207 (2013).
- <sup>21</sup> J.-U. Thiele, S. Maat, J. L. Robertson, and E. E. Fullerton, *IEEE Trans. Magn.* **40**, 2537 (2004).
- <sup>22</sup> J. B. Staunton, R. Banerjee, M. dos Santos Dias, A. Deak, and L. Szunyogh, *Phys. Rev. B* **89**, 054427 (2014).
- <sup>23</sup> R. Cherifi, V. Ivanovskaya, L. C. Phillips, A. Zobelli, I. Infante, E. Jacquet, V. Garcia, S. Fusil, P. Briddon, N. Guiblin, A. Mougin, A. Unal, F. Kronast, S. Valencia, B. Dkhil, A. Barthelemy, and M. Bibes, *Nature Mater.* **13**, 345 (2014).
- <sup>24</sup> J. Junquera and P. Ghosez, *Nature* **422**, 506 (2003).
- <sup>25</sup> V. Garcia and M. Bibes, *Nat. Commun.* **5**, 4289 (2014).
- <sup>26</sup> M. Rayson and P. Briddon, *Comput. Phys. Commun.* **178**, 128 (2008).
- <sup>27</sup> R. Jones and P. Briddon, *Semicond. Semimetals* **51A**, 287 (1998).
- <sup>28</sup> C. Hartwigsen, S. Goedecker, and J. Hutter, *Phys. Rev. B* **58**, 3641 (1998).
- <sup>29</sup> H. J. Monkhorst and J. D. Pack, *Phys. Rev. B* **13**, 5188 (1976).
- <sup>30</sup> L. Bocher, A. Gloter, A. Crassous, V. Garcia, K. March, A. Zobelli, S. Valencia, S. Enouz-Vedrenne, X. Moya, N. D. Marthur, *et al.*, *Nano Lett.* **12**, 376 (2011).
- <sup>31</sup> We find a cell parameters of 2.92 Å and 2.94 Å for AFM FeRh and FM FeRh, respectively, in good agreement with experimental values<sup>1,2</sup>.
- <sup>32</sup> M. Takahashi and R. Oshima, *J. Phys. C8*, 491 (1995).
- <sup>33</sup> R. Oshima, F. Hori, Y. Kibata, M. Komatsu, and M. Kiritani, *Mat. Sci. Eng.* **A350**, 139 (2003).
- <sup>34</sup> M. E. Gruner, E. Hoffmann, and P. Entel, *Phys. Rev. B* **67**, 064415 (2003).
- <sup>35</sup> L. M. Sandratskii and P. Mavropoulos, *Phys. Rev. B* **83**, 174408 (2011).
- <sup>36</sup> R. Gu and V. Antropov, *Phys. Rev. B* **72**, 12403 (2005).
- <sup>37</sup> H. Miyajima and S. Yuasa, *J. Magn. Magn. Mater.* **104–107**, 2025 (1992).
- <sup>38</sup> C.-G. Duan, S. S. Jaswal, and E. Y. Tsymbal, *Phys. Rev. Lett.* **97**, 047201 (2006).
- <sup>39</sup> G. Catalan, *Phase Transitions* **81**, 729 (2008).
- <sup>40</sup> M. L. Medarde, *J. Phys.: Condens. Matter* **9**, 1679 (1997).
- <sup>41</sup> M. Imada, A. Fujimori, and Y. Tokura, *Rev. Mod. Phys.* **70**, 1039 (1998).